PAPER

Check for updates

Barkhausen noise in the organic ferroelectric copolymer P(VDF:TrFE)†

Andrey Alekseevich Butkevich, Marcel Hecker, Toni Seiler and Martijn Kemerink [ID] *

Polarization reversal within a ferroelectric material is commonly described as a progression of smaller switching events, giving rise to crackling or Barkhausen noise. While studies on Barkhausen noise, and particularly the associated event size distribution, allow for better understanding of switching processes in ferroelectrics, they have not yet been conducted experimentally on organic ferroelectric materials. In this work, Barkhausen noise in the organic ferroelectric copolymer poly(vinylidene fluoride-*co*-trifluoroethylene) (P(VDF:TrFE)) is experimentally investigated under different electric fields, increasing at various rates. A weak dependence of the structure of the Barkhausen noise on both the magnitude and rise time of the applied electric field is observed, which manifests as a trend in the probability density function power-law exponents. Specifically, an increase in maximum electric field leads to an increase of the power-law exponent; increasing the rise time causes a parallel shift towards lower exponents. While these findings do not allow to conclusively confirm or refute universal self-organized critical behavior of the polarization reversal avalanches in P(VDF:TrFE), the exponents were found to seemingly converge to the 'universal' value of 1.5 for fast and strong driving, suggesting the system is close to this limit.

1. Introduction

For organic ferroelectrics, it has been established that bistable polarization and hence ferroelectric switching can be achieved by multiple mechanisms, like reorientation of permanent dipoles generating spontaneous polarization (conventional ferro-electrics),[1] donor–acceptor systems (charge-transfer complexes),[2–5] hydrogen-bonded compounds,[6–9] and many others.[10,11] However, insight into how one state changes into another in a bistable system is almost entirely lacking. The present explanations have been mostly derived from theory and developed models.[12–14] While analytical (macroscopic), Monte Carlo (microscopic) and first-principle theory based (density functional theory) models have been applied to describe the ferroelectric switching processes, molecular dynamics have especially been successful in this task.[14–18] In contrast, experimentally measuring and investigating the underlying mechanisms has been proven to be challenging for both inorganic and especially organic materials.[19]

One powerful method to study the process of ferroelectric switching and gain more insight into the cooperativity and the disorder being characteristic of extrinsic switching is the observation of crackling – or Barkhausen – noise, which appears in ferroelectric materials during ferroelectric polarization reversal. It has been investigated and was confirmed during switching processes, although virtually all studies were confined to inorganics and especially perovskites.[20–26] Typically, in such noise spectroscopy experiments, power-law distributions were established for multiple quantities related to the switching processes. While the recovered exponents varied between different materials, the overall similar behavior suggests universality in systems exhibiting Barkhausen noise.[21–23,25,26]

For organic ferroelectric materials, the – to our best knowledge – only experimental investigation into Barkhausen noise was performed by Mai and Kliem on thin films of the well-known organic ferroelectric copolymer poly(vinylidene fluoride-*co*-trifluoroethylene) (P(VDF:TrFE)).[27] In their work, the measured current peaks were generated without an applied electric field due to the thermally-induced reordering of dipoles while crossing the Curie-temperature. Although the Barkhausen pulses only corresponded to the switching of a very small number of dipoles (much less than 1% of total dipoles), clear deviations from a continuous switching process with different shapes were observed.[27] While this study confirmed Barkhausen noise in the copolymer PVDF, it did neither investigate the system through ferroelectric switching nor the power-law behavior. Furthermore, we previously performed a study on the prototypical organic molecular ferroelectric benzene-1,3,5-tricarboxamide (BTA).[28] While we were able to numerically model the BTA system *via* kinetic Monte Carlo simulations, indeed finding Barkhausen noise and strong indications for

Institute for Molecular Systems Engineering and Advanced Materials, Im Neuenheimer Feld 225, Heidelberg, 69120, Germany. E-mail: martijn.kemerink@uni-heidelberg.de

† Electronic supplementary information (ESI) available. See DOI: https://doi.org/10.1039/d5cp00677e

This journal is © the Owner Societies 2025

Phys. Chem. Chem. Phys., 2025, **27**, 9637–9644 | 9637

self-organized criticality, we could not measure the Barkhausen noise experimentally as the number of simultaneously switching dipoles was, in actual agreement with the simulations, not enough to provide measurable currents given the resolution threshold of the used setup. Prior to coming to the specific goals of the present investigation, we will first give a brief overview of relevant previous works on Barkhausen noise and switching kinetics in P(VDF-TrFE).

Physical systems typically exhibit specific length scales, characterizing the events occurring within them. In critical systems, the events occur on all possible length scales. The corresponding critical behavior often gives rise to a power-law distribution of the event sizes, which, however, is not sufficient as the only indicator for critical behavior but should be present in case of one.[29,30] If a power-law occurs in a critical system, the value of the exponent may indicate universality. Barkhausen noise may be used as a probe of such critical behavior. It is the response of a system to the change of external conditions such as electric field, temperature, *etc.* with suddenly appearing and discrete events of varying sizes. In ferroelectric materials, in the vicinity of the coercive field the change of external electric field causes (groups of) dipoles to switch and hence the polarization to change.[25] The resulting events are discrete, can vary widely in size and indeed seem to typically follow a power-law distribution.[31]

In general, not all systems exhibit crackling behavior. Depending on their internal structure, and especially the structural disorder, some respond to external forces with numerous similarly sized and small events, others have typically only few large events as their response. The former is also called popping while the latter is known as snapping. Systems exhibiting crackling noise fall between these two cases based on the interactions within the system, hence representing a transitional behavior between popping and snapping.[31] As such, noise spectroscopy can be used to investigate the internal structure and cooperativity in ferroic materials, with the (relative) strength of disorder determining the spectral distribution of the events – intrinsic switching in an ideal, defect-free ferroelectric would give rise to a single snapping event spanning the entire volume, whereas dominant disorder would wash out any correlations, leading to popping noise.

The mean field plasticity (MFP) model was initially developed for materials under shear stress that display step-like stress–strain curves and exhibit material-independent power-law event size distributions.[32] Similar to how crackling noise can manifest as popping, crackling or snapping, these materials show varied behaviors depending on the coupling of their individual parts. The MFP model assumes that a slip is initiated once the local failure stress τ_f is exceeded and continues until the local stress falls below the sticking stress τ_s. Due to material disorder, both the local failure and sticking stress can vary depending on the location within the material. Furthermore, the initial slip may induce additional slips in adjacent areas as it alters the local stress, hence triggering an avalanche propagating through the material as the external force F gradually increases. This description yields an equation of motion whose solution

predicts, in accordance with the domain wall propagation model, a power-law distribution of all sizes with an exponential cut-off.[33] The theory also describes that the distributions are (stress) integrated over the applied force upon collecting the data over extensive stress ranges.[34] This integration causes the power-law exponents to increase as the largest avalanches occur at the critical stress.[35]

It was shown that the MFP model can also be applied to the switching processes in ferroic materials, in which case the step-like stress–strain curve is to be understood as the step-like motion of a domain boundary, resulting from the competition between, typically, a driving force in the form of an increasing electric field and stopping force associated with pinning at structural defects.[32,36] For ferroic materials, this implies that data collected over the entire hysteresis loop aligns with the stress integrated exponents, whereas data taken solely around the coercive field corresponds to the non-stress integrated values.[35] The resulting critical power-law exponents describing the event size distribution τ and energy distribution ε are 2 and 5/3 for the former and 3/2 and 4/3 for the latter, respectively.[32]

A seemingly unrelated description of the switching kinetics of real, *i.e.* disordered, ferroelectrics is provided by the thermally activated nucleation limited switching (TA-NLS) model that states that switching processes in ferroelectric materials are limited and initiated by the activation of pre-existing small nucleation sites.[37,38] The activation of a nucleation site may be described as the thermally driven polarization reversal of a critical volume V^*, which is then followed by further domain growth. The latter can in principle be left unspecified, but is commonly described by the classical Kolmogorov–Avrami–Ishibashi (KAI) theory that accounts for (continuous) space filling domain growth.[39,40]

The TA-NLS model provides the following expression for the coercive field E_c dependent on the temperature T and the voltage sweeping frequency ν_{exp}:

$$E_c = \frac{w_b}{P_s} - \frac{k_B T}{V^* P_s} \ln\left(\frac{\nu_0}{\nu_{exp} \ln 2}\right) \tag{1}$$

with the energy barrier between two metastable states w_b, the saturation polarization P_s, the Boltzmann factor k_B ($k_B T$ as thermal energy of the system) and the attempt-to-flip frequency associated with the material specific phonon frequency ν_0. A high sweeping frequency in a hysteresis loop measurement leads to a large coercive field since the system cannot equilibrate and fully relax in time. Furthermore, the model predicts that the coercivity of a ferroelectric system increases with the driving frequency since the switching itself becomes more intrinsic, giving rise to more larger and fewer smaller switching events, similar to the behavior of the creep regime. The coercive field decreases linearly with temperature and the logarithm of the inverse frequency, as shown in eqn (1). In another work, we simulated the Barkhausen noise in the organic molecular discotic BTA and concluded that the power-law exponents are anti-correlated to the coercivity of the system.[28]

The TA-NLS model has been applied to the nucleation sites in P(VDF:TrFE) and the critical volume V^* was estimated to be

9638 | *Phys. Chem. Chem. Phys.*, 2025, **27**, 9637–9644

This journal is © the Owner Societies 2025

4 nm^3 in a previous work.[40] As discussed in Section S1 in the ESI,† this volume yields a number of dipoles that is many orders of magnitude below of what can be measured experimentally by noise spectroscopy. Still, the resulting avalanches might be detectable, which is the purpose of the current work. In particular, while the (Preisach) distribution of nucleation sites in P(VDF:TrFE) was previously shown to give insight in how these domains interact, this gives no information about the subsequent polarization reversal cascades. Therefore, it is not clear whether a direct or indirect relation exists between the Preisach and Barkhausen event size distributions.

In this work, we demonstrate experimental measurements of Barkhausen noise in the ferroelectric copolymer P(VDF:TrFE). The measurements are conducted for multiple applied voltages below, at and above the coercive field as well as for three different rise times. The power-law exponents are extracted from the obtained histograms, which are fitted with two different fitting methods. Depending on the rise time, the power-law exponents sit around or slightly below the universal values for critical behavior predicted by the MFP model. Increasing the applied electric field from below to above the coercive field leads to a weak increase of power-law exponents. Longer rise times and hence slower driving shift the power-law exponents to lower values, which agrees with the TA-NLS model. While the trends of the power-law exponents do not suggest universality, they do, for higher fields and faster driving, converge around the estimated value of 1.5, suggesting the system is close to critical; for lower fields and slower driving, the system appears to be in a regime with an abundance of larger 'snapping' events.

2. Samples, data acquisition and analysis procedure

Measurements were carried out on out-of-plane samples with a thin P(VDF:TrFE) film between two crossed gold electrodes. The chemical structure of P(VDF:TrFE) is given in Fig. S2.1a in the ESI.† Both side and top views of a single device are shown in Fig. S2.1b and c in the ESI.† A schematic of the measurement setup is provided in Fig. S2.2 (ESI†) and further experimental details are given in Section 5. Prior to noise measurements, the ferroelectric switching of the samples was checked; a typical result and its explanation are shown in Fig. S2.3 in the ESI.† Values found for the coercive field E_c and remnant polarization P_r were (dependent on frequency, temperature and applied voltage) approximately 20–25 V μm^{-1} and 60–65 mC m^{-2}, respectively, in good agreement with previous results.[41,42] A typical atomic force microscopy (AFM) topography image of a spin coated P(VDF:TrFE) thin film is shown in Fig. S2.4 in the ESI.†

The measuring setup was optimized to provide the lowest possible noise floor with the given devices and is described in some detail in the Section S3 in the ESI.† Every measurement, that is a single combination of applied voltage and rise time, was repeated multiple times for each sample and the data was captured in bundles of 100 current waveforms. The electric field was applied *via* the double wave method (DWM), which is depicted in Fig. S2.3 and S2.5 in the ESI.† In short, the DWM applies a poling pulse twice in every poling direction, allowing to correct for background currents and hence isolate the switching current by subtracting the second signal peak from the first assuming that the first poling peak saturates the switching current for the given electric field strength. Since not all measurements exhibited Barkhausen noise, the data was cleaned up before analysis. For each measurement, the slew-rate $S(t) = \left(\frac{dI}{dt}\right)^2$ was calculated and compared to a threshold based on the maximum applied voltage. If the threshold was not met, the waveforms were rejected. Otherwise, the waveform was displayed and manually approved in order to further sort out spurious signals that appeared semi-randomly, but seemed to become more frequent after prolonged measurement, especially at higher fields. The distinction between true Barkhausen noise and *e.g.* charge trapping and release and breakdown phenomena is discussed in ESI† Section S3 as well. Although this is not pursued further here, we tentatively attribute the disappearance of Barkhausen noise to a gradual decrease of structural disorder due to an effective 'field annealing'. Interestingly and importantly, the appearance or disappearance of the Barkhausen noise signals was not correlated to the overall switching behavior, which continued to correspond to the full polarization reversal, happening around a constant coercive field. An automated approach was explored but was declined due to a high false-positive rate.

The sorted datasets were analyzed by multiple steps. An exemplary analysis process is shown in Fig. 1. First, the calculated slew-rate $S(t) = \left(\frac{dI}{dt}\right)^2$ was considered and datasets with $S < 10^{-5}$ A^2 s^{-2} were excluded. This threshold was based on typical measured results so that most of the background noise was excluded, as shown in Fig. 1b. Next, the baseline was calculated by identifying the local minima of the slew-rate and interpolating these datapoints using the piecewise cubic Hermite interpolating polynomial (PCHIP). The interpolated baseline was subtracted from the calculated slew-rate to account for the underlying slew-rate caused by the slope of the switching peak, as indicated in Fig. 1c. Using the corrected slew-rate, the probability density function (PDF) was calculated. Finally, power-laws were fitted on to the PDFs in double logarithmic representation of the data to obtain the power-law exponents *via* the slope of the fit, as shown in Fig. 1d. For better statistics, two methods were used for the power-law fitting: The maximum likelihood (ML) and the least squares (LS) methods. Details on these fitting methods can be found in Section S2 in the ESI.†

3. Experimental results

Based on previous results, an effect of both the rise time and the applied voltage on the power-law exponents was expected. Thus, the measurements were done for three different rise
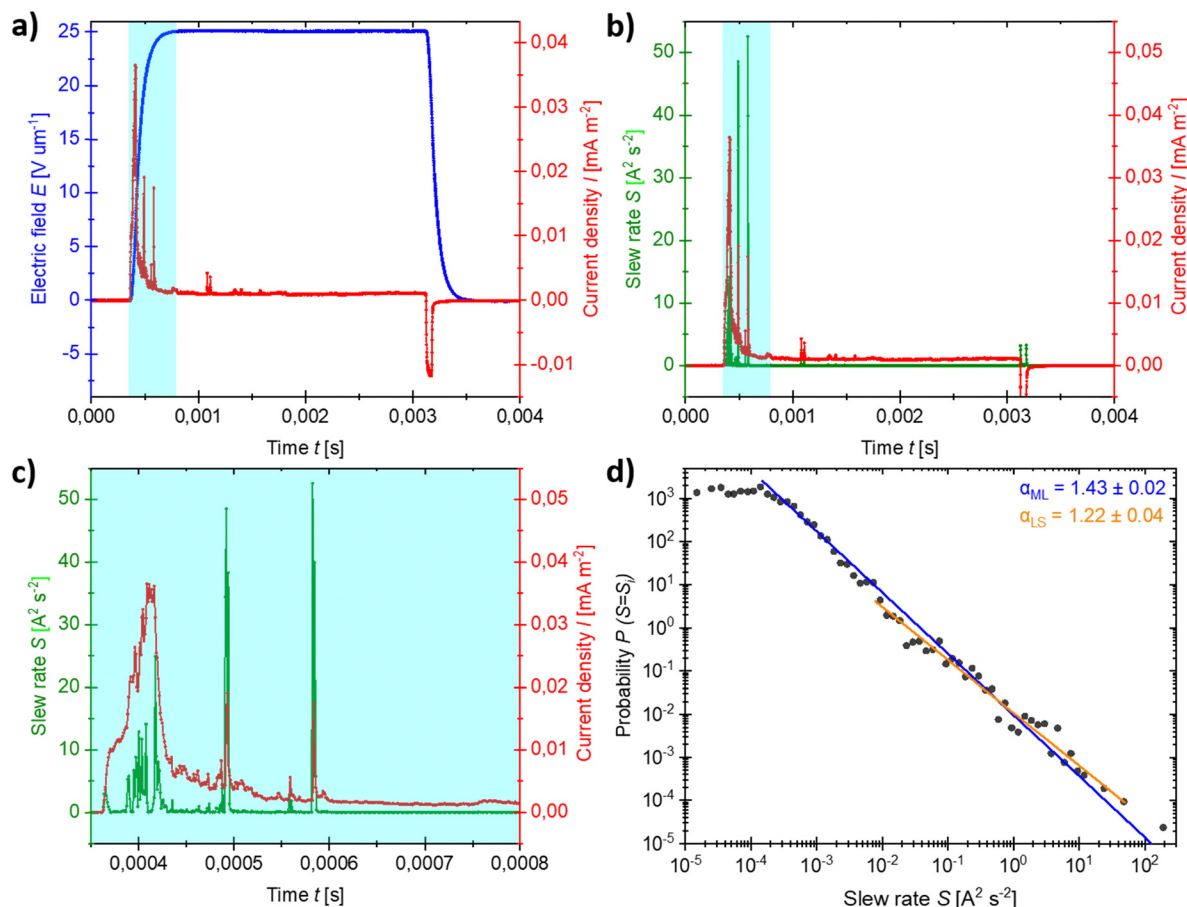
This journal is © the Owner Societies 2025

Phys. Chem. Chem. Phys., 2025, **27**, 9637–9644 | **9639**

Fig. 1 An example of a typical data analysis for an applied voltage of ∼25 V. (a) The measured current density of a P(VDF:TrFE) sample (red) as a response to an applied square electric field waveform (blue). The rising slope of the waveform (marked in cyan) is rounded due to the (input) noise-filtering circuit. The downward peak in the current density at ∼3.2 ms arises from displacement current. The current peaks after the voltage ramp arise as the sample is not fully switched during the ramp, since the applied electric field is near the coercive field. The corresponding P–E-hysteresis loop is shown in Fig. S2.6 in the ESI.† (b) The slew rate S (green) calculated from the current signal (red). (c) The slew rate S (green) and current signal (red) zoomed in on the relevant part of the measured spectrum, which is from the beginning to the end of the applied voltage waveform slope as marked in cyan in (a) and (b). (d) The fitted power-laws with the extracted power-law exponents for the measurement using both ML (blue line) and LS (orange line; depicted as linear) fitting methods.

times, *cf.* Section S3 in the ESI,† while maintaining a constant frequency of the total double-wave pulse train. Likewise, the applied voltage was varied from below to well beyond the coercive field.

The box plot in Fig. 2 summarizes our findings; the underlying histograms for all individual measurements are provided in Section S4 (Fig. S4.2–4) in the ESI† with a measurement of a dielectric reference capacitor provided in Fig. S4.1 (ESI†) for comparison. The variability of the samples during prolonged measurements that was discussed above also led to a significant fraction of non-ideal probability distributions, which inspired the use of two independent approaches, ML and LS, to determine the power law exponents. Apart from a small offset, the two approaches lead to similar values of the mean exponent, slightly below the mean field value of 1.5. In addition, as visible in Fig. 2a, both analysis methods suggest a weak trend of increasing exponents for higher driving speeds (and hence lower rise times), with the 100 µs rise time leading

to values at or close to the 1.5 expected from the mean field plasticity model. The same trend is visible for both fitting methods when plotting the power-law exponents against the applied voltage for the three different rise times, see Fig. 2b. The individual exponent values for different applied voltages and rise times are shown in Fig. S4.6 (ESI†). In addition, higher applied voltages, and hence higher electric fields, lead, for a fixed rise time, to higher power-law exponents with an increase of roughly 0.01 V^{-1}, as indicated by the dashed lines in Fig. S4.6 (ESI†).

The trends in extracted power-law exponents both as a function of rise times and applied voltage suggest that the system is not truly critically self-organized, as no universal behavior seems to be present. However, the power-law exponent values for both fastest (100 µs) and strongest (above coercive field) driving are very close to the mean field value of 1.5, hence indicating that the system is close to such behavior. Furthermore, the distributions in general become more ideal for shorter rise
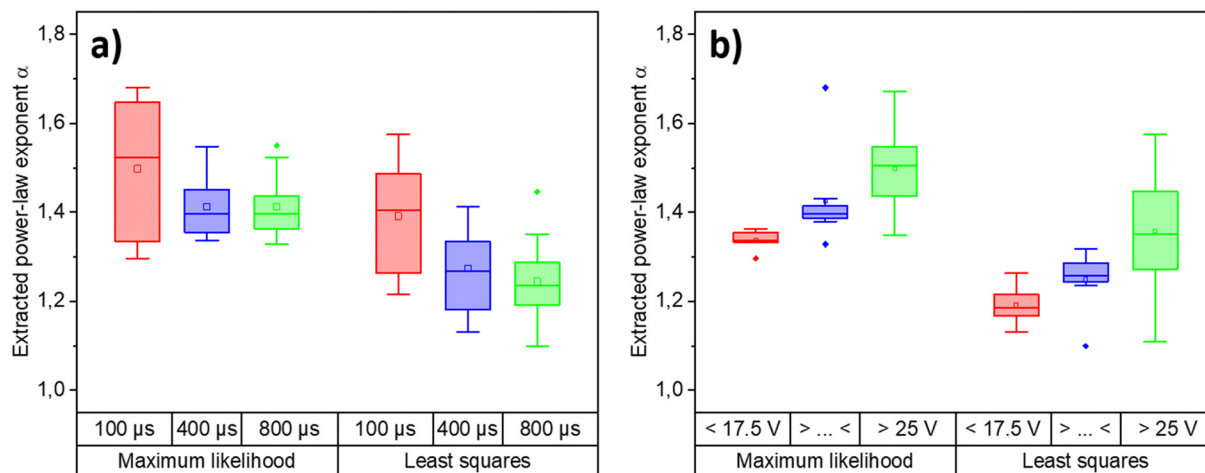
9640 | *Phys. Chem. Chem. Phys.*, 2025, **27**, 9637–9644

This journal is © the Owner Societies 2025

Fig. 2 Box plot of the extracted critical power–law exponents α for (a) three different rise times including all applied voltages for each rise time in the analysis and (b) three different intervals of the applied voltage including all rise times for each voltage interval in the analysis for both fitting methods. The shorthand label of the middle panel indicates voltages between 17.5 and 25 V. Some data points were deemed inconclusive based on the difficulty to obtain unique fits to the histograms and were excluded here. A similar box plot with all values is shown in Fig. S4.5 in the ESI.†

times and higher fields (see Fig. S4.2–4 in the ESI†), which is consistent with the notion that the system approaches self-organized criticality for those conditions. In contrast, the significant variability of the response curves and hence the extracted critical power-law exponents, especially at weaker driving, suggests that the behavior is not universally self-organized and instead depends on minor variations in the structural (dis)order that – for instance – occur upon repeated switching at higher fields. This, in turn, is in line with our observation of an increasing occurrence of spurious signals in prolonged measurements at higher fields, as mentioned previously in Section 2.

Furthermore, the trends in power-law exponents observed in Fig. 2 and Fig. S4.5 and S4.6 (ESI†) are consistent with the TA-NLS model that predicts that increasing rise times, and hence lowering the driving speed, leads to less coercivity in the system, which yields fewer larger and more smaller events, resulting in generally smaller extracted power-law exponents. This is in line with our previous findings for coercivity and the corresponding event sizes within a simulated BTA ferroelectric system.[28] Especially below the coercive field, the extracted power-law exponents are lower than expected from the mean field theory, which agrees with other studies carried-out for magnetic systems and can be explained by the entire system not being fully switched.[43] In that scenario, less stable parts of the system can switch before reaching the coercive field, leading to isolated smaller events that do not progress into larger, system-spanning avalanches and hence to smaller power-law exponents.

As mentioned in Section 1, the TA-NLS theory has previously been used to investigate the (Preisach) distribution of nucleation sites (hysterons) in P(VDF:TrFE), for which a typical critical volume V^* of 4 nm^3, which corresponds to roughly 10^3 switched dipoles, has been established.[40] In our case, the smallest event sizes that can be resolved experimentally correspond to roughly 10^8 dipoles switching simultaneously. As such, the measured signals must reflect the resulting avalanches and not the

nucleation events. Although the absence of specific data does not allow us to draw firm conclusions, we would like to propose a possible connection between the distributions of nucleation sites and switching events, inspired by our numerical work on BTA.[28] In that work, we found that small hysterons, consisting of stacks of ~ 10 molecules each, that are separated from each other by morphological defects, can both act as nuclei for polarization reversal and form the building blocks for system-spanning avalanches. Whether this leads to universal critical behavior depends on the degree of, and variation in, the coupling between these hysterons. In the case of BTA, which is a quasi-1D system consisting of hexagonally packed supramolecular stacks, the maximum event size is nevertheless limited to several hundreds of molecules, that is, the size of a single column. Given its rather different morphology, domain growth in P(VDF:TrFE) may be expected to show a higher dimensionality that supports much larger avalanches that are still built up from much smaller, interacting hysterons,[39,40] which is supported by previous findings where the characteristic geometric dimension for the domain growth in P(VDF:TrFE) becomes generally larger on increasing the driving electric field.[44] While speculative, this may be the underlying mechanism for the herein observed behavior. The avalanches triggered by the small nuclei can, apparently, give rise to critical behavior that is close to self-organized critical. The degree to which that happens depends on how strongly the system is driven and, in view of the significant sample-to-sample variation and the absence of signals after longer operation, seems to depend on relatively subtle variations in morphology.

4. Summary

In this work, the Barkhausen noise associated with polarization reversal in thin film P(VDF:TrFE) samples was experimentally

This journal is © the Owner Societies 2025

Phys. Chem. Chem. Phys., 2025, **27**, 9637–9644 | **9641**

measured for different applied voltages and rise times. The obtained histograms of event sizes were fitted with both the maximum likelihood and least squares fitting methods and the power-law exponents were extracted. The exponents were consistently slightly higher for the former fitting method and below or at the mean field value of 1.5 for both fitting methods. Both decreasing the rise time and increasing the applied voltage led to an increase of the extracted power-law exponents. The trends of the extracted power-law exponents have been identified as consistent with the thermally-assisted nucleation-limited switching (TA-NLS) model. Based on the trends, it has been concluded that the system is not truly critically self-organized due to the lack of universal behavior. However, as the exponents for both the fastest rise time and applied voltages above the coercive field were close to the mean field value and the corresponding distributions became more ideal, it seems that the system approached self-organized criticality for those conditions. For weaker and slower driving, the behavior is not universally self-organized and instead depends on variations in structural (dis)order that varies between samples and even during measurements. Lastly, on basis of their magnitude, the measured Barkhausen noise cannot directly be mapped upon the distribution of nucleation sites in the TA-NLS model was deemed impossible. Instead, we speculate that the domain growth in P(VDF:TrFE) progresses through avalanches that are built up from larger numbers of such sites, with an interaction that strongly depends on sample morphology and (switching) history.

5. Experimental details

5.1. Measurement setup

The input signal was supplied by a Keysight 33600A arbitrary waveform generator (AFG) and amplified by a TReK PZD350A high voltage amplifier. Considerations and tests that were performed to select these devices are provided in Section S3 in the ESI.† The device response was measured by either a Zurich Instruments impedance analyzer (MFIA) or lock-in amplifier (MFLI). No significant differences between the MFIA and MFLI were established. The device under test was measured inside a Linkam miniature cryostat featuring electric contacts to reduce noise and allow for precise temperature dependent measurements. All Barkhausen noise measurements were performed at room temperature.

5.2. Sample preparation

Out-of-plane electrodes were used for device fabrication of thin film P(VDF:TrFE) samples. Commercially available Corning plain microscope slides with a thickness of 0.96 to 1.06 mm were cut and both bottom and top electrodes were thermally evaporated. Gold (on chromium in case of bottom) electrodes of different thicknesses (typically 50–70 nm) were utilized. The P(VDF:TrFE) thin films (PVDF:TrFE 77%:23% commercially supplied by Solvay and used as received) were statically spin coated on top of the bottom electrodes with 900 rpm from a 60 mg mL^{-1} PVDF:TrFE in cyclohexanone (solvent supplied by VWR chemicals; ≥99.0% purity) solution, which was stirred overnight and filtered before spin coating, with 150 µl solution deposited per sample at room temperature. The deposited films were additionally annealed at 140 °C for two hours to promote crystallinity in the ferroelectric β-phase, which yielded typical film thicknesses of ∼300–400 nm. Each sample consisted of a total of nine devices. Three different electrode widths were used for both top and bottom contacts (0.2, 0.5 and 1 mm), so that each sample included all possible nine combinations of bottom and top electrode widths. The results for the different electrode combinations were consistent, although combinations of larger electrode widths were significantly more prone to short-circuits. A total of 144 crossbar out-of-plane samples were tested, of which most were short-circuited and 32 showed Barkhausen noise.

5.3. Surface characterization

The film thicknesses and the corresponding roughness were determined *via* a stylus profilometer (Bruker DektakXT). The high-resolution surface images were obtained *via* a Bruker MultiMode 8-HR atomic force microscope operated in tapping mode.

Data availability

The data supporting this article have been included as part of the manuscript and its ESI.†

Conflicts of interest

The authors declare no conflicts of interest.

Acknowledgements

References

1 C. F. C. Fitié, W. S. C. Roelofs, P. C. M. M. Magusin, M. Wübbenhorst, M. Kemerink and R. P. Sijbesma, Polar Switching in Trialkylbenzene-1,3,5-tricarboxamides, *J. Phys. Chem. B*, 2012, **116**, 3928–3937.

2 S. Horiuchi, T. Hasegawa and Y. Tokura, Molecular Donor–Acceptor Compounds as Prospective Organic Electronics Materials, *J. Phys. Soc. Jpn.*, 2006, **75**, 051016.

3 S. Horiuchi, K. Kobayashi, R. Kumai and S. Ishibashi, Ionic versus Electronic Ferroelectricity in Donor–Acceptor Molecular Sequences, *Chem. Lett.*, 2014, **43**, 26–35.

9642 | *Phys. Chem. Chem. Phys.*, 2025, **27**, 9637–9644

This journal is © the Owner Societies 2025

4 S. Horiuchi, S. Ishibashi and Y. Tokura, in *Organic Ferro-electric Materials and Applications*, ed. K. Asadi, Woodhead Publishing, 2022, pp. 7–46.

5 S. Barman, A. Pal, A. Mukherjee, S. Paul, A. Datta and S. Ghosh, Supramolecular Organic Ferroelectric Materials from Donor–Acceptor Systems, *Chem. – Eur. J.*, 2024, **30**, e202303120.

6 Z. Sun, T. Chen, C. Ji, S. Zhang, S. Zhao, M. Hong and J. Luo, High-Performance Switching of Bulk Quadratic Nonlinear Optical Properties with Large Contrast in Polymer Films Based on Organic Hydrogen-Bonded Ferroelectrics, *Chem. Mater.*, 2015, **27**, 4493–4498.

7 S. Horiuchi and S. Ishibashi, Hydrogen-Bonded Small-Molecular Crystals Yielding Strong Ferroelectric and Anti-ferroelectric Polarizations, *J. Phys. Soc. Jpn.*, 2020, **89**, 051009.

8 J. Wu, Q. Zhu, T. Takeda, N. Hoshino and T. Akutagawa, Ferroelectricity of Hydrogen-Bonded Azobenzene Deriva-tives, *ACS Appl. Electron. Mater.*, 2021, **3**, 3521–3529.

9 S. Horiuchi, S. Ishibashi and Y. Tokura, in *Organic Ferro-electric Materials and Applications*, ed. K. Asadi, Woodhead Publishing, 2022, pp. 47–84.

10 S. Horiuchi and Y. Tokura, Organic ferroelectrics, *Nat. Mater.*, 2008, **7**, 357–366.

11 H. Liu, Y. Ye, X. Zhang, T. Yang, W. Wen and S. Jiang, Ferroelectricity in organic materials: from materials char-acteristics to de novo design, *J. Mater. Chem. C*, 2022, **10**, 13676–13689.

12 T. D. Cornelissen, M. Biler, I. Urbanaviciute, P. Norman, M. Linares and M. Kemerink, Kinetic Monte Carlo simula-tions of organic ferroelectrics, *Phys. Chem. Chem. Phys.*, 2019, **21**, 1375–1383.

13 T. D. Cornelissen, I. Urbanaviciute and M. Kemerink, Micro-scopic model for switching kinetics in organic ferroelectrics following the Merz law, *Phys. Rev. B*, 2020, **101**, 214301.

14 T. Cornelissen and M. Kemerink, in *Organic Ferroelectric Materials and Applications*, ed. K. Asadi, Woodhead Publish-ing, 2022, pp. 185–232.

15 J. Liu, W. Chen, B. Wang and Y. Zheng, Theoretical Methods of Domain Structures in Ultrathin Ferroelectric Films: A Review, *Materials*, 2014, **7**, 6502–6568.

16 M. Sepliarsky, A. Asthagiri, S. R. Phillpot, M. G. Stachiotti and R. L. Migoni, Atomic-level simulation of ferroelectricity in oxide materials, *Curr. Opin. Solid State Mater. Sci.*, 2005, **9**, 107–113.

17 R. E. Cohen, in *Ferroelectricity*, John Wiley & Sons, Ltd, 2005, pp. 139–154.

18 U. V. Waghmare, First-Principles Theory, Coarse-Grained Models, and Simulations of Ferroelectrics, *Acc. Chem. Res.*, 2014, **47**, 3242–3249.

19 A. Picinin, M. H. Lente, J. A. Eiras and J. P. Rino, Theoretical and experimental investigations of polarization switching in ferroelectric materials, *Phys. Rev. B: Condens. Matter Mater. Phys.*, 2004, **69**, 064117.

20 V. Y. Shur, E. L. Rumyantsev, D. V. Pelegov, V. L. Kozhevnikov, E. V. Nikolaeva, E. L. Shishkin, A. P. Chernykh

and R. K. Ivanov, Barkhausen Jumps During Domain Wall Motion in Ferroelectrics, *Ferroelectrics*, 2002, **267**, 347–353.

21 I. S. Baturin, M. V. Konev, A. R. Akhmatkhanov, A. I. Lobov and V. Y. Shur, Investigation of Jerky Domain Wall Motion in Lithium Niobate, *Ferroelectrics*, 2008, **374**, 136–143.

22 V. Y. Shur, A. R. Akhmatkhanov, I. S. Baturin and E. V. Shishkina, Polarization reversal and jump-like domain wall motion in stoichiometric LiTaO$_3$ produced by vapor trans-port equilibration, *J. Appl. Phys.*, 2012, **111**, 014101.

23 C. D. Tan, C. Flannigan, J. Gardner, F. D. Morrison, E. K. H. Salje and J. F. Scott, Electrical studies of Barkhau-sen switching noise in ferroelectric PZT: Critical exponents and temperature dependence, *Phys. Rev. Mater.*, 2019, **3**, 034402.

24 C. Flannigan, C. D. Tan and J. F. Scott, Electrical studies of Barkhausen switching noise in ferroelectric lead zirconate titanate (PZT) and BaTiO3: critical exponents and temperature-dependence, *J. Phys.: Condens. Matter*, 2019, **32**, 055403.

25 E. K. H. Salje, D. Xue, X. Ding, K. A. Dahmen and J. F. Scott, Ferroelectric switching and scale invariant avalanches in BaTiO$_3$, *Phys. Rev. Mater.*, 2019, **3**, 014415.

26 B. Casals, G. F. Nataf and E. K. H. Salje, Avalanche criticality during ferroelectric/ferroelastic switching, *Nat. Commun.*, 2021, **12**, 345.

27 M. Mai and H. Kliem, Observation of thermal Barkhausen effect in ferroelectric films of poly(vinylidene fluoride/trifluoroethylene) copolymer, *J. Appl. Phys.*, 2013, **114**, 224104.

28 A. A. Butkevich, F. T. Thome, T. Seiler, M. Hecker and M. Kemerink, *Barkhausen noise in the columnar hexagonal organic ferroelectric BTA*, arXiv, 2024, preprint, arXiv: arXiv:2412.12666, DOI: **10.48550/arXiv.2412.12666**.

29 K. G. Wilson, Problems in Physics with Many Scales of Length, *Sci. Am.*, 1979, **241**, 158–179.

30 D. Sornette, *Critical Phenomena in Natural Sciences: Chaos, Fractals, Selforganization and Disorder: Concepts and Tools*, Springer Science & Business Media, 2006.

31 J. P. Sethna, K. A. Dahmen and C. R. Myers, Crackling noise, *Nature*, 2001, **410**, 242–250.

32 K. A. Dahmen, Y. Ben-Zion and J. T. Uhl, Micromechanical Model for Deformation in Solids with Universal Predictions for Stress-Strain Curves and Slip Avalanches, *Phys. Rev. Lett.*, 2009, **102**, 175501.

33 K. A. Dahmen, in *Avalanches in Functional Materials and Geophysics*, ed. E. K. H. Salje, A. Saxena and A. Planes, Springer International Publishing, Cham, 2017, pp. 19–30.

34 M. Zaiser, B. Marmo and P. Moretti, in *Proceedings of International conference on Statistical Mechanics of Plasticity and Related Instabilities—PoS(SMPRI2005)*, Sissa Medialab, Indian Institute of Science, Bangalore, India, 2006, p. 053.

35 G. Durin and S. Zapperi, The role of stationarity in magnetic crackling noise, *J. Stat. Mech.: Theory Exp.*, 2006, **2006**, P01002.

36 E. K. H. Salje and K. A. Dahmen, Crackling Noise in Dis-ordered Materials, *Annu. Rev. Condens. Matter Phys.*, 2014, **5**, 233–254.

This journal is © the Owner Societies 2025

Phys. Chem. Chem. Phys., 2025, **27**, 9637–9644 | **9643**

37 M. Vopsaroiu, J. Blackburn, M. G. Cain and P. M. Weaver, Thermally activated switching kinetics in second-order phase transition ferroelectrics, *Phys. Rev. B: Condens. Matter Mater. Phys.*, 2010, **82**, 024109.

38 M. Vopsaroiu, P. M. Weaver, M. G. Cain, M. J. Reece and K. B. Chong, Polarization dynamics and non-equilibrium switching processes in ferroelectrics, *IEEE Trans. Ultrason. Eng.*, 2011, **58**, 1867–1873.

39 A. V. Gorbunov, T. Putzeys, I. Urbanavičiūtė, R. A. J. Janssen, M. Wübbenhorst, R. P. Sijbesma and M. Kemerink, True ferroelectric switching in thin films of trialkylbenzene-1,3,5-tricarboxamide (BTA), *Phys. Chem. Chem. Phys.*, 2016, **18**, 23663–23672.

40 I. Urbanavičiūtė, T. D. Cornelissen, X. Meng, R. P. Sijbesma and M. Kemerink, Physical reality of the Preisach model for organic ferroelectrics, *Nat. Commun.*, 2018, **9**, 4409.

41 N. Meng, R. Mao, W. Tu, X. Zhu, R. M. Wilson, E. Bilotti and M. J. Reece, Processing and characterization of free standing highly oriented ferroelectric polymer films with remarkably low coercive field and high remnant polarization, *Polymer*, 2016, **100**, 69–76.

42 I. Urbanaviciute, *Multifunctional Supramolecular Organic Ferroelectrics*, Linköping University Electronic Press, 2019.

43 J. P. Sethna, K. A. Dahmen and O. Perkovic, *Random-Field Ising Models of Hysteresis*, arXiv, 2005, preprint, arXiv:arXiv:cond-mat/0406320, DOI: **10.48550/arXiv.cond-mat/0406320**.

44 W. J. Hu, D.-M. Juo, L. You, J. Wang, Y.-C. Chen, Y.-H. Chu and T. Wu, Universal Ferroelectric Switching Dynamics of Vinylidene Fluoride-trifluoroethylene Copolymer Films, *Sci. Rep.*, 2014, **4**, 4772.

9644 | *Phys. Chem. Chem. Phys.*, 2025, **27**, 9637–9644

This journal is © the Owner Societies 2025